electronics

MDPI

Article

A Hybrid Contrast and Texture Masking Model to Boost High Efficiency Video Coding Perceptual Rate-Distortion Performance

Javier Ruiz Atencia [1,*], Otoniel López-Granado [1,*], Manuel Pérez Malumbres [1], Miguel Martínez-Rach [1], Damian Ruiz Coll [2], Gerardo Fernández Escribano [3] and Glenn Van Wallendael [4]

[1] Department Computer Engineering, Miguel Hernández University, 03202 Elche, Spain; mels@umh.es (M.P.M.); mmrach@umh.es (M.M.-R.)
[2] Department of Signal and Communications Theory, Rey Juan Carlos University, 28933 Madrid, Spain; druizcoll@ofinno.com
[3] School of Industrial Engineering, University of Castilla-La Mancha, 13001 Albacete, Spain; gerardo.fernandez@uclm.es
[4] IDLab-MEDIA, Ghent University—IMEC, B-9052 Ghent, Belgium; glenn.vanwallendael@ugent.be
* Correspondence: javier.ruiza@umh.es (J.R.A.); otoniel@umh.es (O.L.-G.); Tel.: +34-96665-8392 (O.L.-G.)

Abstract: As most of the videos are destined for human perception, many techniques have been designed to improve video coding based on how the human visual system perceives video quality. In this paper, we propose the use of two perceptual coding techniques, namely contrast masking and texture masking, jointly operating under the High Efficiency Video Coding (HEVC) standard. These techniques aim to improve the subjective quality of the reconstructed video at the same bit rate. For contrast masking, we propose the use of a dedicated weighting matrix for each block size (from 4×4 up to 32×32), unlike the HEVC standard, which only defines an 8×8 weighting matrix which it is upscaled to build the 16×16 and 32×32 weighting matrices (a 4×4 weighting matrix is not supported). Our approach achieves average Bjøntegaard Delta-Rate (BD-rate) gains of between 2.5% and 4.48%, depending on the perceptual metric and coding mode used. On the other hand, we propose a novel texture masking scheme based on the classification of each coding unit to provide an over-quantization depending on the coding unit texture level. Thus, for each coding unit, its mean directional variance features are computed to feed a support vector machine model that properly predicts the texture type (plane, edge, or texture). According to this classification, the block's energy, the type of coding unit, and its size, an over-quantization value is computed as a QP offset (DQP) to be applied to this coding unit. By applying both techniques in the HEVC reference software, an overall average of 5.79% BD-rate gain is achieved proving their complementarity.

Keywords: HEVC; perceptual coding; HVS; CSF; texture masking; contrast masking; MDV; SVM; adaptive QP

Citation: Atencia, J.R.; López-Granado, O.; Pérez Malumbres, M.; Martínez-Rach, M.; Coll, D.R.; Fernández Escribano, G.; Van Wallendael, G. A Hybrid Contrast and Texture Masking Model to Boost High Efficiency Video Coding Perceptual Rate-Distortion Performance. *Electronics* **2024**, *13*, 3341. https://doi.org/10.3390/electronics13163341

Academic Editor: Krzysztof Okarma

Received: 27 May 2024
Revised: 6 August 2024
Accepted: 17 August 2024
Published: 22 August 2024

1. Introduction

Image and video compression standards play an essential role in modern media communication, enabling the efficient storage and transmission of digital content. However, the compression process unavoidably introduces some degree of information loss, resulting in image or video distortion that can be perceived by human observers. To improve the subjective quality of compressed media, many techniques based on the perception of the human visual system (HVS) have been developed.

The quantization stage is a crucial step in the image and video coding chain, where information is discarded to reduce the quantity of data to be stored or transmitted. This process introduces artifacts and distortions that are not present in the original source. Therefore, it is crucial to consider the limitations and properties of the HVS to develop efficient compression algorithms.

The masking properties of the HVS have been extensively studied to provide mechanisms to quantize the information of image areas where reconstruction errors are not perceived by the HVS [1]. The HVS is not always able to detect distortions when they are masked by texture, contrast, luminance, and other factors. Therefore, these masking properties can be used to reduce the perceptual impact of compression artifacts.

Contrast masking is one of the most commonly used HVS-based techniques to reduce compression artifacts. It involves incorporating the contrast sensitivity function (CSF) during the quantization stage of image and video codecs. The CSF shows that the HVS is unable to detect differences between objects and their background under certain conditions of luminance, distance, or spatial frequency [2–6]. Compression artifacts can be masked under these conditions because they function as foreground, while the scene acts as the background.

Texture and luminance masking are two techniques that also exploit properties of the HVS to reduce compression artifacts. Texture masking takes advantage of the fact that the presence of texture in some areas of the image can mask some of the reconstruction errors, making it more difficult to detect a compression artifact in a textured area than in a homogeneous one. On the other hand, luminance masking is based on the observation that compression artifact errors are less noticeable in areas with high or low luminance. This means that errors in dark or bright regions of an image are less visible to the HVS, allowing for the reduction in the amount of information to be encoded without significant perceptual loss.

The rest of this paper is structured as follows. In Section 2, the state of the art is presented. The proposed contrast and texture masking models for the HEVC video coding standard are explained in Section 3. Section 4 gives the results when masking techniques are applied to a series of well-known video sequences. Finally, Section 5 summarizes the conclusions of this study and makes some recommendations for future research.

2. Related Work

Tong et al. [7] proposed a perceptual model of texture and luminance masking for images compressed using the JPEG standard [8]. The authors provided a method to classify the transform blocks according to their content type, namely, texture blocks (containing a lot of spatial activity), edge blocks (containing a clear edge as primary feature) or plain blocks (generally smooth, with low spatial activity). The authors claimed that human sensitivity to error was, in general, inversely proportional to the spatial activity, and was extremely sensitive to low spatial activity areas (plain blocks). To perform this classification, the authors used an algorithm that was based on the weight of the Discrete Cosine Transform (DCT) coefficients grouped by their frequency or position within the transformed block. Finally, the degree of additional quantization that should be applied to each block was determined in such a way that the distortions produced by increments in quantization remained masked.

Tong's model has been modified and refined by other authors. For example, Zhang et al. [9] built a luminance model and block classifier using the mean of the DCT coefficients. Zhang et al. also considered the intra-band masking effect, which refers to the imperceptible error tolerance within the sub-band itself. In other words, a different quantization value is applied for each coefficient within the 8×8 block, depending on the block classification and the coefficient position in the block.

Most models are based on partitioning the image into 8×8 blocks [9–11], however Ma et al. [12] extended the classification algorithm to block sizes of 16×16 to adapt for higher image resolutions. Furthermore, the proposed classification model was performed in the pixel domain. This was based on the Canny edge detector and applied an adaptive quantization scheme that depended on the block size. The problem of edge detection algorithms lies in finding the optimal threshold value: choosing a low value causes very small edges to be detected, while choosing a high value skips important edges [13]. Several authors [14,15] used a 4×4 reduction of the classifier proposed in [7].

Regarding video coding standards, several studies have incorporated perceptual coding schemes in their reference software. In MPEG-2 Test Model 5 [16], a quantization parameter (QP) offset based on the spatial activity is defined, which is calculated as a function of the variance of pixels within the macroblock. Tang et al. [17] proposed a bit allocation technique for the JM7.6 reference software of the H.264/AVC video coding standard by adopting a novel visual distortion sensitivity model that was based on motion attention and texture structure.

From version 16 of the HEVC reference software encoder description [18], there has been an option called adaptive QP that varies the quantization parameter for each coding unit (CU) to provide improved perceptual image quality. This algorithm is based on the algorithm used in MPEG-2 TM5. Prangnell et al. [19] proposed a modified version of the adaptive QP algorithm by extending the spatial activity calculation to the chrominance channels and obtained better performance than when using only the luminance. In [20], Kim et al. designed a perceptual video coding scheme for HEVC based on Just Noticeable Differences (JND) models, including contrast, texture, and luminance masking, in both transform and pixel domains. JND models are based on determining the threshold under which the HVS is unable to perceive differences from the original source. The main drawback of [20] is that the behavior of the rate-distortion optimization (RDO-based) mode decision is modified, and therefore, corrective factors are required to compensate for the distortion introduced by JND.

Wang et al. [21] proposed a block-level adaptive quantization (BLAQ) for HEVC, where each CU had its own QP adapted to the local content. The authors did not use masking techniques to determine the QP; instead, it was obtained by a brute-force algorithm. To reduce the complexity of the algorithm, the authors modified the rate-distortion cost function that gives priority to the distortion, as measured in the Peak Signal-to-Noise Ratio (PSNR). Xiang et al. proposed in [22] a novel adaptive perceptual quantization method based on an adaptive perceptual CU early-splitting algorithm to address the spatial activity and Lagrange multiplier selection problems in the HEVC quantization method. In [23], Zhang et al. proposed a method to predict the optimal QP value at the Coding Tree Unit (CTU) level by employing spatial and temporal combined masks using the perception-based video metric (PVM). Because the default CTU block size is 64×64, this work did not take advantage of HEVC's quadtree partitioning when applying masking techniques in smaller regions.

Recent advancements in the development of contrast masking models using deep learning have been reported in literature. Marzuki et al. [24] proposed an HEVC perceptual adaptive quantization based on a deep neural network. They determined the QP at the frame level and therefore did not take advantage of texture masking in scenes with multiple texture types. Bosse et al. [25] proposed a method of distortion-sensitive bit allocation in image and video compression based on distortion sensitivity estimated using a deep Convolutional Neural Network (CNN). Sanagavarapu et al. [26] explored the use of Region of Interest (ROI) techniques by segmenting the surgical incision region and encoding it with the complexity-efficient scalable HEVC, highlighting the application of perceptual algorithms to improve bit rate efficiency while maintaining visual quality in surgical telementoring systems.

An important aspect to be considered when including masking in an encoder is the way that the block type or the adaptive quantization value to be applied in each block is signaled in the bitstream. Most of the cited authors use the thresholds that are defined by the JND model to discard the coefficients below a certain value (i.e., being included in the image or video encoding algorithm) without sending additional information to the decoder. In [7], Tong et al. analyzed the performance of both methods, namely the first method that does not send extra information and the second method that requires extra side information to be sent to the decoder. They concluded that the latter method achieved a better rate-distortion (RD) performance. Studies that are based on modifying the QP

value at the slice or block level often make use of the delta QP parameter, which is the difference between the current QP and the previously encoded QP.

Many of the works that have been cited so far make use of the PSNR distortion metric to evaluate the RD performance. However, it is well-known that the PSNR metric does not accurately reflect the perceptual assessment of quality [27,28]. Consequently, in studies, such as [12], subjective tests were conducted using the Difference Mean Opinion Score (DMOS) as an indicator of perceptual quality. However, given that the PSNR is not an adequate metric to properly evaluate the impact of perceptual techniques, we decided to use some objective metrics that attempt to characterize the subjectivity of the HVS, such as Structural Similarity (SSIM) [29], Multi-Scale SSIM (MS-SSIM) [30], and PSNR-HVS-M [31], to measure their RD performance.

The SSIM and the MS-SSIM metrics are based on the hypothesis that the HVS is highly adapted to extract structural information from the scenes. Both metrics consider the luminance, contrast, and structural information of the scenes, whereas MS-SSIM also considers the scale. The PSNR-HVS-M metric, which is a modified version of PSNR, considers the contrast sensitivity function and the between-coefficient contrast masking of DCT basis functions.

In this work, we present a novel scheme of texture and contrast masking to be applied in the HEVC reference software [18]. For the contrast masking model, we start from the frequency-dependent quantization matrices that are included in the HEVC reference software for blocks from 8×8 to 32×32 sizes. In addition, we add a new 4×4 weighting matrix [32] that achieves an additional rate reduction while maintaining the perceptual quality. For the texture masking model, we make use of the mean directional variance (MDV) metric, and we use a support vector machine (SVM) to perform the block classification (plain, edge, or texture). The QP offset value is calculated as a function of the block classification and its texture energy, in a similar way as that proposed by Tong et al. [7].

To demonstrate the potential of this novel scheme, we encode a set of well-known test sequences and analyze their performance in terms of rate and distortion. The results are presented with the BD-rate model [33], using the SSIM, MS-SSIM, and PSNR-HVS-M distortion metrics.

The main innovations provided by this work are the following ones:

- An improved contrast masking method that covers all HEVC available block sizes (4×4 to 32×32) that includes a new efficient quantization matrix;
- A new block classification method for block texture masking based on the MDV metric that efficiently classifies every block as a texture, edge, or plain block;
- A new QP offset calculator for the HEVC adaptive QP tool, based on the block texture energy and its classification.

All these innovations define a novel perceptual quantizer based on the one proposed in the HEVC reference software.

3. Proposed HEVC Perceptual Quantizer

In this section, the details of the new perceptual quantizer for the HEVC video coding standard is described. We first describe how CSF masking is applied in HEVC (scaling list tool) followed by the proposed improvements. Then, after applying the CSF masking, we use a texture masking over-quantization scheme that is based on (a) the use of a new block classifier, and (b) an optimized over-quantizer that depends on the block type and its energy.

3.1. Proposed Contrast Sensitivity Function

Contrast masking is a perceptual compression technique that exploits the visual adaptation of the HVS to contrast. This adaptation depends on the amount of contrast between an object and its surroundings (or background), the distance, and the spatial frequency. Several studies have been performed to characterize the CSF using subjectively measured human contrast thresholds for different spatial frequencies [3,5,6]. In this regard,

the Mannos and Sakrison model [2] and the Daly model [4] are among the most popular in the field of image and video coding.

The HEVC standard uses a frequency-dependent quantization to implement CSF masking [34]. Depending on its contrast sensitivity importance, a different amount of quantization is applied to each frequency coefficient of a block (i.e., the higher the perceptual importance, the lower the corresponding quantization level).

With this goal in mind, the HEVC reference software defines the use of static non-uniform quantization matrices, which are also called weighting matrices, by setting the `ScalingList` (SCL) option to 1 (default is 0) in the coding configuration parameters. These weighted quantization matrices are defined for the intra- and interpredictions, as well as for the luminance component and the chrominance components. In terms of CUs, non-uniform quantization matrices are only defined for CUs of 8×8 (see Figure 1b). Meanwhile, for 16×16 and 32×32, the matrices are obtained by upsampling, using a replication of the 8×8 matrix. In the case of 4×4 CUs, the HEVC reference software does not define any weighting matrix, and therefore it uses a uniform matrix (see Figure 1a).

$$\begin{bmatrix} 16 & 16 & 16 & 16 \\ 16 & 16 & 16 & 16 \\ 16 & 16 & 16 & 16 \\ 16 & 16 & 16 & 16 \end{bmatrix}$$

(**a**) Default 4×4 quantization weights (intra- and interprediction)

$$\begin{bmatrix} 16 & 16 & 16 & 16 & 17 & 18 & 21 & 24 \\ 16 & 16 & 16 & 16 & 17 & 19 & 22 & 25 \\ 16 & 16 & 17 & 18 & 20 & 22 & 25 & 29 \\ 16 & 16 & 18 & 21 & 24 & 27 & 31 & 36 \\ 17 & 17 & 20 & 24 & 30 & 35 & 41 & 47 \\ 18 & 19 & 22 & 27 & 35 & 44 & 54 & 65 \\ 21 & 22 & 25 & 31 & 41 & 54 & 70 & 88 \\ 24 & 25 & 29 & 36 & 47 & 65 & 88 & 115 \end{bmatrix}$$

(**b**) Default 8×8 quantization weights (intraprediction)

Figure 1. Default HEVC quantization weighting matrices.

In this work, we include a new 4×4 weighting matrix to increase the compression level for small blocks while maintaining the same perceptual quality. Instead of deriving the matrix weights by downsampling the default quantization matrix of size 8×8, as the standard does for the higher-resolution matrices, we propose to determine the weights of the 4×4 matrix from the study presented in [32]. The author proposes the use of the CSF model of Daly [4] (Equation (1)), where f is the radial frequency in cycles/degree (cpd), assuming the best viewing conditions in which defects are detected earlier. In other words, using a high-resolution display and a short viewing distance. Coding or compression defects may be masked by the content and by the visual capacity at higher resolution and longer viewing distance.

$$H(f) = 2.2(0.192 + 0.114 \cdot f) \cdot e^{-(0.114 \cdot f)^{1.1}} \tag{1}$$

In order to determine the maximum frequency represented in the signal (f_{max}), we begin by calculating the sampling frequency (f_s) using Equation (2). The maximum frequency is then given by Equation (3).

$$f_s = \frac{v \cdot \tan(1^\circ) \cdot r}{0.0254} \tag{2}$$

$$f_{max} = \frac{f_s}{2} \tag{3}$$

Assuming a display resolution of $r = 600$ pixels per inch (ppi) and a viewing distance $v = 12.23$ inches, the maximum frequency is $f_{max} = 64.04$. The CSF curve obtained with Equation (1) is shown in Figure 2.

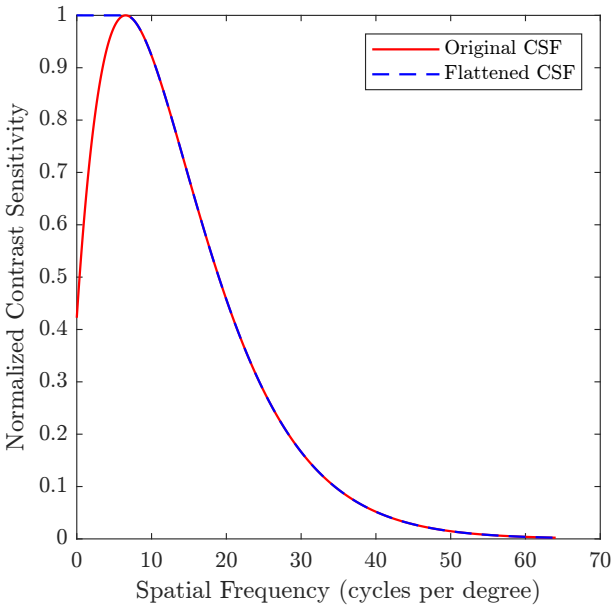

Figure 2. Contrast sensitivity function. The red curve represents the original CSF as defined by Equation (1), while the blue dashed curve represents the flattened CSF, with spatial frequencies below the peak sensitivity saturated.

The red curve corresponds to the definition of the CSF according to Equation (1). As we can see, the HVS is most sensitive in an intermediate region, acting as a bandpass filter, while it is less sensitive to very low and very high frequencies. In addition, as shown with the blue dashed curve in Figure 2, spatial frequency values below the maximum sensitivity peak have been saturated. This is done to preserve the information of the coefficients close to the DC component and including it, because it is in that region where most of the information (energy) is concentrated after applying the DCT to a block.

Using the CSF model of Daly [4], the CSF curve is calculated as shown in Equation (1). This curve represents the sensitivity of the HVS to different spatial frequencies. Each coefficient in the 4×4 DCT block corresponds to a specific spatial frequency. The frequency $f(u, v)$ for each coefficient (u, v) is calculated by considering the horizontal and vertical frequencies of the DCT basis functions. The radial frequency $f(u, v)$ is given by Equation (4).

$$f(u, v) = \sqrt{u^2 + v^2} \tag{4}$$

where $u, v \in 0, 1, 2, 3$. The calculated frequencies are then mapped onto the CSF curve to get the sensitivity values. These values represent how sensitive the HVS is to the corresponding frequencies in the DCT block. The sensitivity values are scaled and normalized to obtain the final weighting values. The scaling ensures that the weights are appropriately adjusted to maintain perceptual quality while increasing compression efficiency. The normalization step involves scaling the values such that the smallest value is 16 and the largest value is scaled to match the highest weight used in the HEVC standard matrices. Finally, the proposed 4×4 weighting matrices are obtained (Figure 3).

$$\begin{bmatrix} 16 & 16 & 20 & 32 \\ 16 & 17 & 21 & 37 \\ 20 & 21 & 29 & 55 \\ 32 & 37 & 55 & 115 \end{bmatrix} \qquad \begin{bmatrix} 16 & 16 & 19 & 29 \\ 16 & 17 & 20 & 32 \\ 19 & 20 & 26 & 46 \\ 29 & 32 & 46 & 91 \end{bmatrix}$$

(**a**) Intraprediction (**b**) Interprediction

Figure 3. Proposed 4×4 quantization weighting matrices for intra- and interprediction modes.

For the remaining block sizes, we use the default weighting matrices that were proposed by the HEVC standard. To implement our proposal in the HEVC reference software, we set the ScalingList parameter to 2. This allows us to define a custom weighting matrix scheme from a text file, which is identified by the ScalingListFile parameter.

To measure the impact of this optimization, we conducted an experimental test using the HEVC reference software version 16.20 [35]. The test video sequences (see Table 1 and Appendix A) from the HEVC conformance test proposal [36] were encoded with the SCL parameter set to 1 (default weighting matrices) and 2 (custom weighting matrix scheme), and the gains (BD rate) were obtained and compared to the default encoding (SCL set to 0). The other coding tools were left with their default values, with the exception of the transform skip (TransformSkip) parameter, which was disabled for all sequences except those of class F to maximize the perceptual response, as stated in [37].

Table 1. HEVC video test sequence properties.

Class	Sequence Name	Resolution	Frame Count	Frame Rate	Bit Depth
A	Traffic	2560 × 1600	150	30	8
	PeopleOnStreet		150	30	8
	Nebuta		300	60	10
	SteamLocomotive		300	60	10
B	Kimono	1920 × 1080	240	24	8
	ParkScene		240	24	8
	Cactus		500	50	8
	BQTerrace		600	60	8
	BasketballDrive		500	50	8
C	RaceHorses	832 × 480	300	30	8
	BQMall		600	60	8
	PartyScene		500	50	8
	BasketballDrill		500	50	8
D	RaceHorses	416 × 240	300	30	8
	BQSquare		600	60	8
	BlowingBubbles		500	50	8
	BasketballPass		500	50	8
E	FourPeople	1280 × 720	600	60	8
	Johnny		600	60	8
	KristenAndSara		600	60	8
F	BaskeballDrillText	832 × 480	500	50	8
	ChinaSpeed	1024 × 768	500	30	8
	SlideEditing	1280 × 720	300	30	8
	SlideShow		500	20	8

The average BD-rate performance (negative values mean gains) for different perceptual metrics is shown in Table 2. Low BD-rate gains were achieved (always below 1%) by enabling only the weighting matrices included in the HEVC standard (SCL = 1). Even for low-resolution sequences (classes C and D), BD-rate losses were observed for some metrics, such as for SSIM metric in class D sequences, where a loss of 1.26% was introduced.

Table 2. Average coding performance [% BD rate] when using our proposed 4 × 4 weighting matrix (intraprediction).

Sequence Class	SCL = 1 (HEVC Presets)			SCL = 2 (Ours)		
	SSIM	MS-SSIM	PSNR- HVS-M	SSIM	MS-SSIM	PSNR-HVS-M
Class A	−0.66	−0.33	−0.62	−1.06	−0.82	−1.58
Class B	−0.97	−0.48	−0.99	−3.20	−2.58	−4.23
Class C	0.26	0.08	−0.08	−4.82	−5.36	−7.39
Class D	1.26	0.29	−0.05	−1.36	−5.66	−7.65
Class E	−0.74	−0.50	−0.75	−1.78	−1.39	−1.98
Class F	−0.15	−0.04	−0.11	−4.57	−4.19	−4.17
Average	−0.17	−0.16	−0.43	−2.80	−3.33	−4.48

As shown in Table 2 (SCL = 2), our proposal obtained a remarkable increase in BD-rate gains for all cases. The improvement was between 2.64% and 4.05% on average for all classes. The SSIM metric scores were lower when compared to the other metrics on low-resolution video sequences (classes C and D), while PSNR-HVS-M obtained the highest BD-rate gains (above 7.39%) for these sequences. Meanwhile, there seemed to be a consensus on all metrics for class E (video-conference applications) and F (synthetic or artificial) sequences because they all obtained broadly similar results.

In Figure 4, we can see that our proposal reduced the bit rate considerably as the quantization parameter decreased, in other words, at low compression rates. This occurred because as the value of the quantization parameter was reduced, the number of TUs (transform units) of size 4 × 4 increased, and thus, the performance impact of our proposed 4 × 4 weighting matrix was more noticeable.

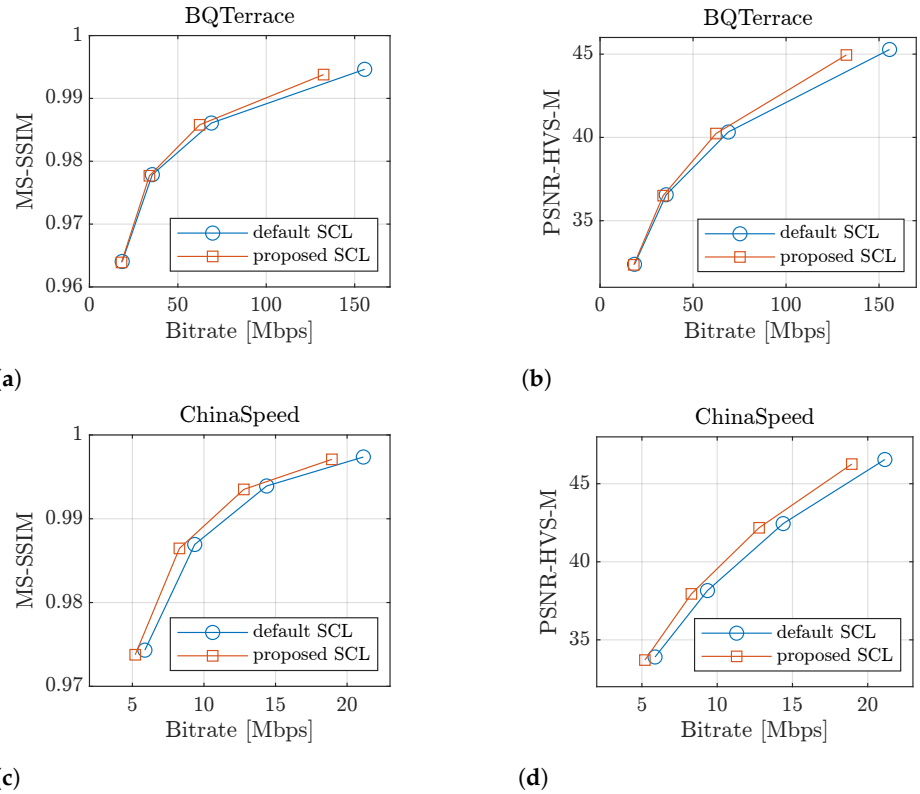

Figure 4. Rate-distortion curves comparing our proposed CSF with the default implemented in the HEVC standard using different perceptual metrics. (**a**,**b**) correspond to the BQTerrace sequence of class B, while (**c**,**d**) correspond to the ChinaSpeed sequence of class F.

3.2. Block Classification Based on Texture Orientation and SVM

After applying the improved CSF masking, we proceed to compute the proper QP offset based on the block texture information. For this purpose, we first need to identify the texture info of each block by means of a block classifier in a similar way to what Tong et al. [7] proposed for the JPEG image encoder. In [7], the authors stated that to maximize perceptual RD, plain blocks should not be over-quantized; the edge blocks could be minimally over-quantized and texture blocks could be over-quantized according to their texture energy level.

The main limitation when importing the texture classifier scheme that was proposed by Tong et al. into the HEVC standard is the adaptation to the different block sizes. JPEG only uses 8 × 8 block size, whereas HEVC includes a wide variety of CU sizes. It should also be considered that the HEVC standard uses the integer transform (I-DCT and I-DST) of the prediction residual. For those reasons, we propose a novel texture block classification using a supervised SVM, which uses the features obtained from the MDV metric proposed by Damian et al. [38] as input features.

Our first step was the classification of about 1800 HEVC-encoded luma blocks of different sizes, depending on whether they were smooth, edged, or textured. To achieve this, we randomly selected blocks from some image databases, such as the ESPL Synthetic Image Database [39], USC-SIPI Image Database [40], TESTIMAGE [41] and Kodak image dataset [42]. To avoid bias in human classification, five different video coding researchers participated in the classification process. The users classified the blocks according to their type (texture, plane, or edge) by using software that randomly presented the blocks for classification. As an example, Figure 5 shows several manually classified blocks that are organized according to size and block type. As can be seen, the blocks that were classified as plain have a smooth content. In contrast, the content of the texture blocks exhibits a more random pattern. The blocks classified as edge have a very pronounced directionality.

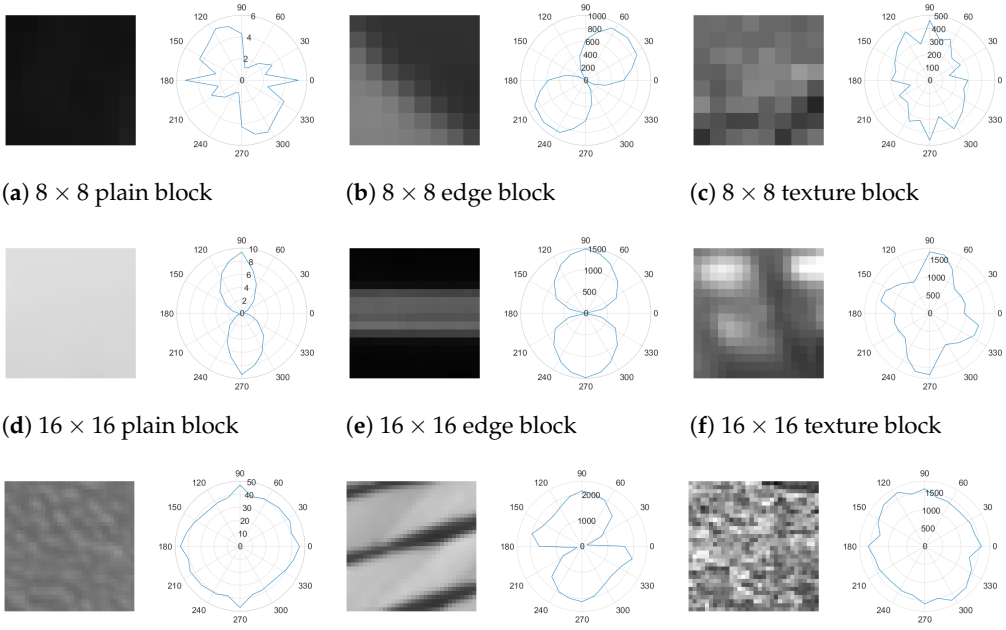

(**a**) 8 × 8 plain block (**b**) 8 × 8 edge block (**c**) 8 × 8 texture block

(**d**) 16 × 16 plain block (**e**) 16 × 16 edge block (**f**) 16 × 16 texture block

(**g**) 32 × 32 plain block (**h**) 32 × 32 edge block (**i**) 32 × 32 texture block

Figure 5. Samples of manually classified blocks (left-hand side) and their associated polar diagram of the MDV metric (right-hand side). From top to bottom: 8 × 8, 16 × 16, and 32 × 32 block sizes; from left- to right-hand side: plain, edge, and texture blocks.

Figure 5 also shows the polar diagram of the MDV values for each block. This metric measures the local directionality of an image by calculating the cumulative variance along discrete lines in the given direction. Using the version of MDV that was introduced in [38],

we computed the twelve rational slopes of all the manually classified blocks to find any correlation between the values of this metric and the classification result. Because the 4×4 block size did not provide sufficient resolution to calculate the 12 rational slopes, and even the manual classification performed by human observers was not completely coherent, the 4×4 blocks were discarded from the texture over-quantization process.

Interesting results can be extracted from the experiments and results shown in Figure 5. On the one hand, texture blocks tended to exhibit polar diagrams that were close to circular shapes, which showed high variance values in all directions. However, edge blocks had a minimum (dominant gradient) in the direction of the edge orientation. Strong edges in a block had higher differences between the minimum and maximum MDV values and were used to form a polar diagram with an "8" shape. Plain blocks tended to have a variety of patterns; however, all of them had relatively very low MDV values when compared to texture and edge blocks (see Figure 5a,d,g).

To establish a robust block classification, we decided to use an SVM classifier. A SVM is a machine learning technique that facilitates linear and non-linear binary classification. Because we wanted to get three block clusters (plane, edge, and texture), we had to use either of two multi-class methods: One vs. One (OvO) or One vs. Rest (OvR). The main difference between these two techniques lies in the number of binary classifier models required. In the OvR strategy, the multi-class classification is split into one binary classification model per class, while for the OvO strategy, for the N-class instances dataset, $(N(N-1))/2$ binary classification models are needed. Because we had only three clusters, both techniques required the same number of binary classification models, and therefore both strategies had similar computational costs.

After analyzing the results of applying different statistics to the MDV data (e.g., the mean, the variance, the median, etc.), it was observed that the best results (i.e., a better clustering in the $\mathbb{R}^3$ space) were obtained using the mean, the variance, and the minimum value of the MDV as the input features to be used in the SVM algorithm. The manual classification of 16×16 blocks of the training dataset is shown in Figure 6a. Texture occupies the YZ plane (they have low $var(MDV)$), edge blocks occupy the XY plane (they have low $min(MDV)$), and plain blocks stay close to the origin of coordinates.

Given that the available block sizes in the HEVC standard are limited, instead of using the block size as an additional feature of a single SVM model, we decided to use one SVM model for each block size.

SVM models were implemented and trained using the Classification Learner application from MATLAB R2020a. The optimizable support vector machine was selected to find the optimal SVM model parameters, including kernel function type (linear, quadratic, cubic, or Gaussian), kernel scale, box constraint, and multi-class method (OvO and OvR).

The optimal parameters and resulting model accuracy of the three models (after 30 iterations of Bayesian optimization) are shown in Table 3. As can be seen, a high degree of accuracy was obtained for all the models, which was sufficient for correct block classification. Figure 6b shows the classification of 16×16 blocks belonging to the testing dataset. It can be seen that the model properly classified the blocks into texture, edge, or plain.

As a visual example, Figure 7 shows the result of applying block classification to the CUs of a BasketballDrill frame quantized at QP 32. It can be seen that the lines of the basket court were correctly labeled as edge blocks, while some parts of the basket net were considered as texture blocks.

Table 3. Optimized SVM models: parameters and accuracy.

Model Parameters	Block Size		
	8 × 8	**16 × 16**	**32 × 32**
Kernel function	linear	linear	linear
Kernel scale	auto	auto	auto
Box constraint level	85	285	35
Multi-class method	One-vs.-All	One-vs.-One	One-vs.-All
Standardize data	true	true	true
Model accuracy	93.9%	95.4%	94.5%

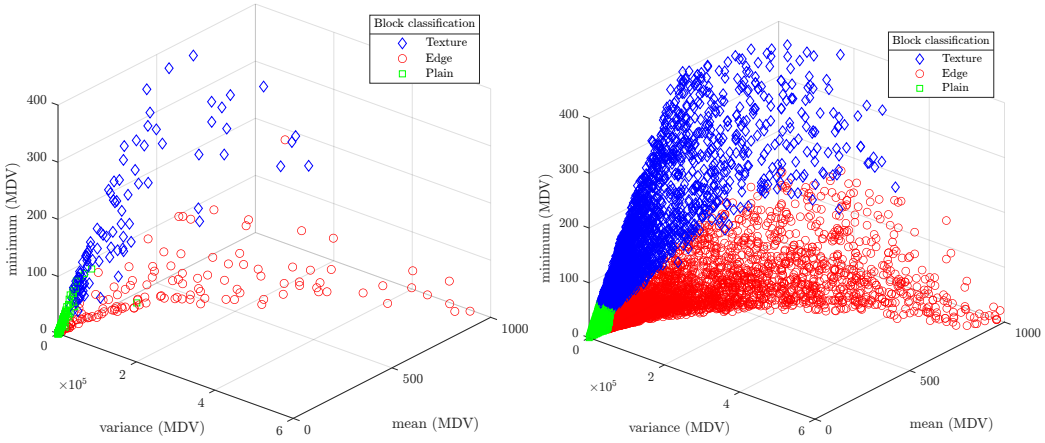

(**a**) Training dataset (**b**) Testing dataset

Figure 6. (**a**) Scatter plot of manually classified 16 × 16 blocks (training dataset), and (**b**) the classification results provided by the trained SVM model (testing dataset)

To integrate the trained SVM models into the HEVC reference software (HM) for evaluation, we exported the trained SVM models from MATLAB to C++. In the HM code, block classification is computed at the frame level before the quadtree partitioning and RDO stage, similar to the adaptive QP algorithm of the HEVC video coding standard [18]. The SVM model inference was performed using the exported C++ code to ensure compatibility and efficiency within the HM framework.

The workflow of the block classification code is as follows: after loading and storing the original YUV pictures into the picture buffer list, if texture masking is enabled, then the function `xPreanalyzeTextureMasking` is called. This function splits each frame into square blocks of size 32, 16, and 8 pixels, the classification of each one is calculated using the corresponding SVM model according to its size. The result is stored in memory. It also calculates and stores the block energy (ε) (defined in Section 3.3), which is required to compute the over-quantization (QP offset). Later, during the partitioning and RDO stage, the block type and energy of each CU are already available according to its size and location inside the frame.

3.3. Obtaining optimal QP offset

The next step after classifying a CU block is to obtain its optimal QP offset. We defined the block energy (ε) as the absolute sum of all of the AC-transformed coefficients of the original picture. The energy distribution was analyzed according to the block type (texture, edge, or plain) and its size. In Figure 8, the block energy distribution is shown as a box plot for each block size and type. This representation allowed us to graphically visualize the five-number summary, which consisted of the minimum and maximum range values, the upper and lower quartiles, and the median.

(**a**) Original BasketballDrill frame

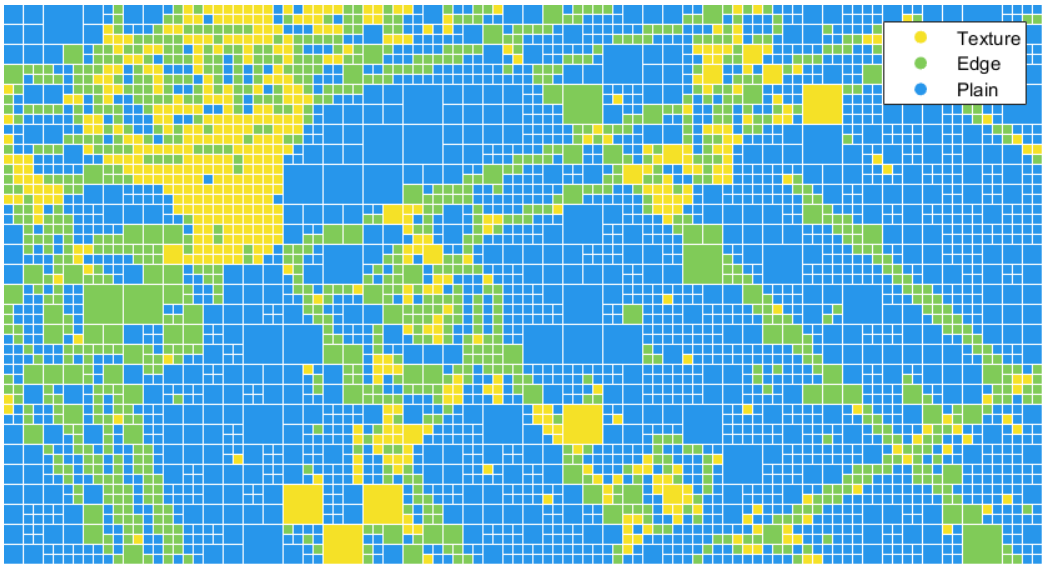

(**b**) Block classification using QP = 32

Figure 7. Example of block classification for the first frame of sequence BasketballDrill, using optimal SVM models for each block size.

A pattern can be observed in terms of the block energy distribution according to the block classification. As expected, blocks classified as texture have the highest block energy distribution, followed by edge blocks and finally, plain blocks have the lowest energy distribution. The outliers in Figure 8 result from synthetic, computer-generated sequences, which exhibit high energy in the middle and high bands. These differ from the majority of blocks from natural sequences in our dataset, explaining the appearance of these extreme cases as outliers.

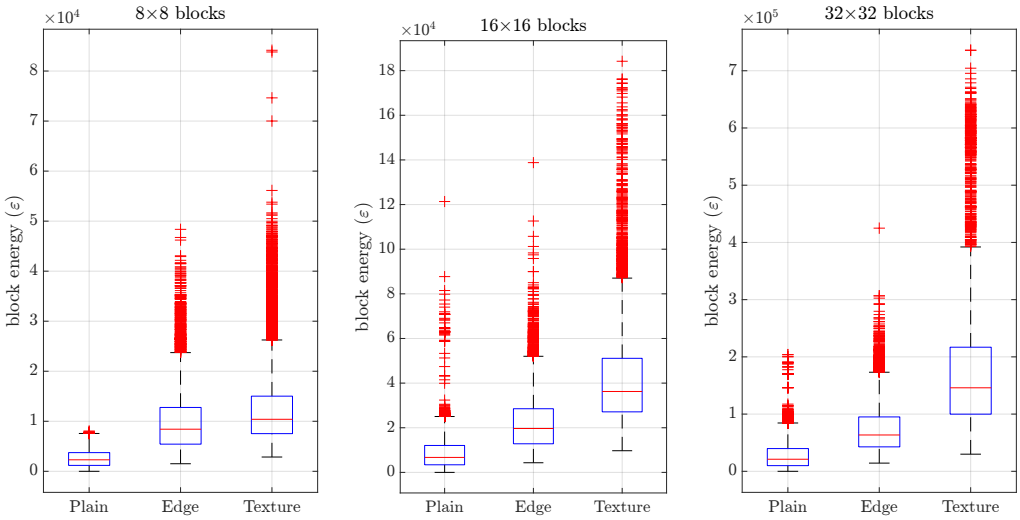

(**a**) 8 × 8 block size (**b**) 16 × 16 block size (**c**) 32 × 32 block size

Figure 8. Box and whisker plot of the block energy (ε) distribution by size and texture classification.

$$\Delta QP_{i,j} = \left\lfloor \frac{6 \cdot \ln(QStep_{i,j})}{\ln(2)} \right\rfloor \tag{5}$$

$$QStep_{i,j} = \begin{cases} 1 & \text{if } \varepsilon(B_{i,j}) \leq MinE, \\ MaxQStep & \text{if } \varepsilon(B_{i,j}) \geq MaxE, \\ 1 + \frac{MaxQStep-1}{MaxE-MinE} \times & \\ (\varepsilon(B_{i,j}) - MinE) & \text{otherwise} \end{cases} \tag{6}$$

In the HEVC standard, the adaptive QP mode assigns to each CU a QP offset or ΔQP that modifies the slice QP adaptively by means of a rate-distortion analysis where PSNR is the distortion metric. Our objective was to also obtain a ΔQP for each CU but we followed a different approach based on the block energy. The distortion metric that we used was perceptually based (e.g., SSIM, MS-SSIM, or PSNR-HVS-M metric).

Equation (5) shows the inverse procedure to obtain ΔQP, as proposed in [43], where $QStep_{i,j}$ is the quantization step size for the CU block $B_{i,j}$ in the block partitioning map, and $\Delta QP_{i,j}$ is the QP offset parameter to be applied to over-quantize the $B_{i,j}$ block. When $QStep_{i,j} = 1$, then $\Delta QP_{i,j} = 0$ (i.e., no additional quantization should be applied to the $B_{i,j}$ block).

To obtain the $QStep_{i,j}$ value for a block, we used the linear threshold elevation function that was presented in Equation (6), similarly to the one proposed in [7], where $MaxE$ and $MinE$ correspond to the maximum and minimum block energy of the set of blocks belonging to the same block type and size (Figure 8), $MaxQStep$ is the maximum allowed quantization step size, $\varepsilon(B_{i,j})$ is the energy of the current block $B_{i,j}$, and $QStep_{i,j}$ corresponds to the quantization step to be assigned to the block. Figure 9 shows the representation of Equation (6), where the two lines show how the slope of the function varies for two different sets of function parameters (i.e., $MinE$, $MaxE$, and $MaxQStep$). As we can see in Figure 9, the corresponding $QStep_{i,j}$ is different for each parameter set, while the block energy $\varepsilon(B_{i,j})$ is the same. The question that arises here is how to choose the function parameters to maximize the overall BD rate [33] performance value. The BD rate was computed by considering the use of a perceptual distortion metric instead of the PSNR.

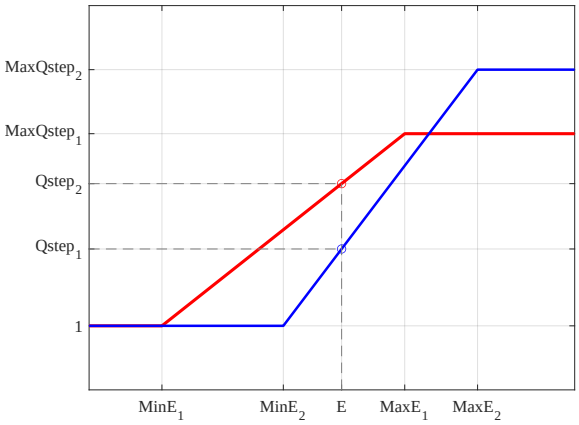

Figure 9. Representation of Equation (6) for two sets of function parameter, (**red**) $MinE_1$, $MaxE_1$ and $MaxQStep_1$ and (**blue**) $MinE_2$, $MaxE_2$, and $MaxQStep_2$. $\Delta QStep_{i,j}$ is different for each set.

We used different sets of parameters to find the optimum combination for each block size (i.e., 8×8, 16×16 and 32×32) and for each block type (i.e., texture and edge). We did not consider plain blocks because they are more sensitive to visible artifacts [7] and should not be over-quantized.

Figure 10 summarizes all the tested parameter sets for each block size and type. A parameter set is built by following the connection arrows in the graph. For example, in the first set, $MinE$ receives the value of the energy at the lower whisker (i.e., 0th percentile), $MaxE$ receives the energy at the bottom of the box (i.e., 25th percentile), and finally the value 1.1 is given to $MaxQStep$. The second parameter set has the same values for $MinE$ and $MaxE$, but we change $MaxQStep$ to 1.2, and so on. To guarantee that the range of the resulting $\Delta QP_{i,j}$ is bounded between 0 and 7 (maximum QP offset allowed in HEVC), we restricted the $MaxQStep$ range to be between 1.1 and 2.5.

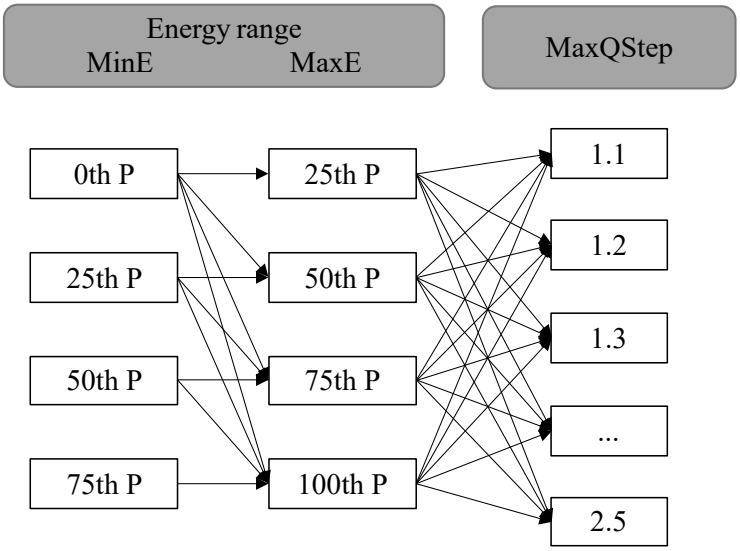

Figure 10. Flowchart of candidate selection for brute-force analysis of perceptually optimal parameters. The Ps in energy range boxes refer to the percentile.

We used the BD rate [33] as a performance metric to determine the best parameter set. Therefore, for each one, we ran a set of encodings using QP values 22, 27, 32, and 37 with the video test sequences belonging to classes A, B, and E which had the highest frame resolution (as suggested in [36]).

After collecting all of the results, we determined the near optimal *MaxE*, *MinE*, and *MaxElevation* values for each block type and size, as in Table 4.

Table 4. Optimal linear function parameters.

Classification	Parameter	Block Size		
		8 × 8	**16 × 16**	**32 × 32**
Texture	MinE	2864	9712	29,952
	MaxE	26,256	26,800	216,880
	MaxElevation	1.3	1.2	2.2
Edge	MinE	1520	4320	14,320
	MaxE	5424	52,016	63,504
	MaxElevation	1.2	1.3	1.2

As an example, applying the optimum parameter set for texture blocks of size 8 × 8 in the PeopleOnStreet video test sequence is shown in Figure 11. This figure shows the evolution of the BD rate (lower is better) for different values of the *MaxQStep* parameter. Each curve corresponds to a certain block energy range (*MinE* and *MaxE* parameters). It can be seen that, for this particular case, the energy range from the 0th to 25th percentile (purple curve with circle marks) obtains the highest BD-rate gain when $MaxElevation = 1.3$.

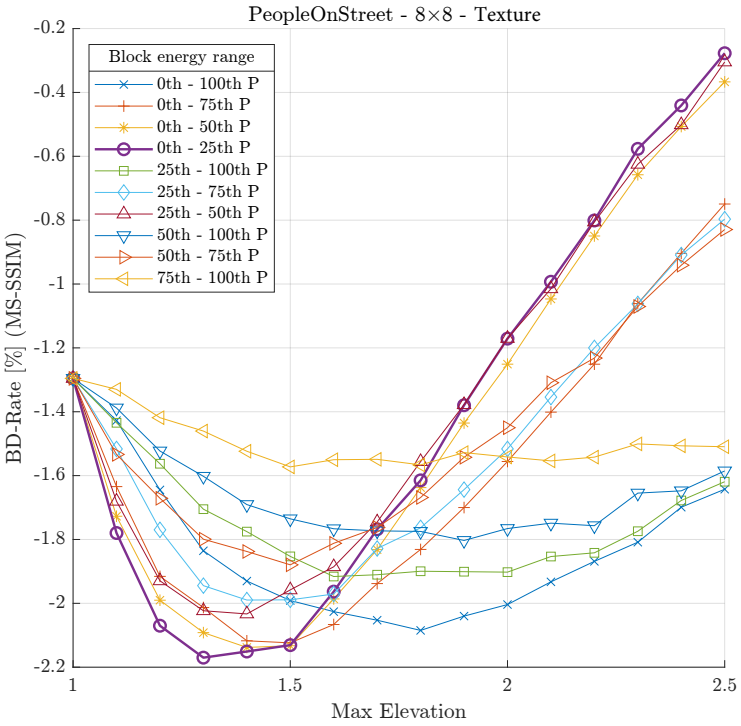

Figure 11. BD-rate curves (MS-SSIM metric) for PeopleOnStreet video test sequence over the *MaxQStep* parameter when modifying texture blocks of size 8. Each curve represents a different block energy range (*MinE* and *MaxE*).

The BD-rate performance for all of the objective quality metrics used after applying the optimal parameters is shown in Table 5. Each column shows the results of applying the optimal over-quantization values only to blocks of the corresponding block type and size.

Table 5. Average coding performance [% BD rate] after applying the optimal $\Delta QP_{i,j}$ values derived from our texture masking proposal.

Class	Metric	Texture Blocks			Edge Blocks		
		8 × 8	16 × 16	32 × 32	8 × 8	16 × 16	32 × 32
A	SSIM	−1.04	−0.98	−1.01	−0.67	−1.07	−1.05
	MS-SSIM	−0.87	−0.76	−0.80	−0.46	−0.80	−0.82
	PSNR-HVS-M	−1.69	−1.44	−1.52	−1.26	−1.52	−1.57
B	SSIM	−3.74	−3.14	−3.15	−3.03	−3.21	−3.19
	MS-SSIM	−3.02	−2.47	−2.52	−2.34	−2.56	−2.57
	PSNR-HVS-M	−4.58	−4.05	−4.17	−3.90	−4.16	−4.21
E	SSIM	−2.12	−1.74	−1.77	−1.48	−1.87	−1.78
	MS-SSIM	−1.68	−1.35	−1.40	−0.98	−1.50	−1.39
	PSNR-HVS-M	−2.14	−1.89	−1.96	−1.17	−2.02	−1.99

4. Results and Discussion

To analyze the behavior of our HEVC perceptual quantizer proposal as a whole, we performed an exhaustive evaluation of the contrast and texture masking models that were described in the previous sections. Following the recommendations defined in the HEVC conformance test [36], we employed (a) all video test sequences proposed, grouping the results by the classes they belonged to (see Table 1) and (b) the BD-rate metric [33] using the SSIM, MS-SSIM, and PSNR-HVS-M as the perceptual video quality metrics. QP values of 22, 27, 32, and 37 were used to compute the BD rate.

The implementation of our proposed contrast and texture masking models was deployed using the HEVC reference software version 16.20 [35], running on a high-performance Linux server with an x86_64 architecture. The server was powered by two Intel® Xeon® Gold 6140 CPU @ 2.30GHz, each with 18 cores. The system was equipped with 376 GB of RAM.

To make texture masking compliant with the HEVC standard (in other words, to make the resulting bitstream readable with any HEVC-compliant decoder), we signaled the corresponding QP offset values at the CU level because the HEVC standard allows the transmission of a delta QP value for each CU block, that is, the difference in QP steps relative to the slice of QP that it belongs to [43].

Tables 6–8 show the results after encoding the whole set of video test sequences for all intra-, random-access, and low-delay coding configurations, respectively. In these tables, the "Contrast masking" column shows the gains that were obtained by applying only our CSF proposal presented in Section 3.1, while the "Contrast and Texture masking" column shows the total gains wgen applying the CSF and texture masking proposals, as explained in Section 3.3.

As expected, applying both contrast and texture masking techniques gave higher gains than applying contrast masking alone. For both of the structural information-based metrics (i.e., SSIM and MS-SSIM), the difference between using or not using texture masking implied an average BD-rate reduction of 1.92% for all intra- (AI), 3.02% for random-access (RA), and 3.44% for low-delay (LD) configurations. Regarding the PSNR-HVS-M metric, the benefit achieved by adding texture masking scheme was lower, with an average BD-rate reduction of 0.82%, 1.64%, and 1.91% for AI, RA, and LD, respectively. It seems that this metric does not take into special consideration the effect of texture masking generated by over-quantizing blocks with higher energy.

Table 6. Average coding performance in all of the intra-configurations [% BD rate].

Class	Sequence Name	Contrast Masking			Contrast and Texture Masking		
		SSIM	MS-SSIM	PSNR-HVS-M	SSIM	MS-SSIM	PSNR-HVS-M
A	Traffic	−1.00	−0.93	−1.77	−2.25	−1.89	−2.05
	PeopleOnStreet	−1.23	−1.27	−1.95	−3.38	−2.98	−2.54
	Nebuta	−1.22	−0.39	−1.64	−2.40	−1.70	−1.85
	SteamLocomotiveTrain	−0.80	−0.67	−0.98	−0.05	−0.04	−0.36
	Average	−1.06	−0.82	−1.58	−2.02	−1.65	−1.70
B	Kimono	−0.50	−0.41	−0.89	−0.53	−0.35	−0.81
	ParkScene	−2.26	−1.67	−3.11	−3.82	−2.91	−3.75
	Cactus	−2.97	−2.26	−4.06	−5.10	−3.94	−4.83
	BQTerrace	−6.68	−5.44	−7.82	−9.61	−8.09	−8.89
	BasketballDrive	−3.61	−3.11	−5.27	−5.05	−4.31	−5.66
	Average	−3.20	−2.58	−4.23	−4.82	−3.92	−4.79
C	RaceHorses	−4.80	−5.60	−7.62	−7.60	−8.21	−9.07
	BQMall	−3.28	−3.53	−4.96	−5.09	−5.26	−5.58
	PartyScene	−6.51	−7.45	−9.89	−8.22	−9.19	−10.75
	BasketballDrill	−4.70	−4.86	−6.58	−7.46	−7.66	−7.86
	Average	−4.82	−5.36	−7.26	−7.09	−7.58	−8.31
D	RaceHorses	−0.63	−3.00	−5.71	−2.43	−5.67	−6.91
	BQSquare	−2.81	−9.24	−10.12	−6.25	−14.24	−12.30
	BlowingBubbles	−0.28	−6.16	−9.39	−1.33	−7.74	−9.87
	BasketballPass	−1.74	−4.25	−5.39	−3.65	−7.07	−6.84
	Average	−1.36	−5.66	−7.65	−3.41	−8.68	−8.98
E	FourPeople	−1.54	−1.27	−1.81	−2.75	−2.25	−1.98
	Johnny	−1.65	−1.00	−1.87	−2.98	−2.25	−1.85
	KristenAndSara	−2.15	−1.88	−2.26	−4.42	−3.87	−2.98
	Average	−1.78	−1.39	−1.98	−3.38	−2.79	−2.27
F	BasketballDrillText	−4.74	−4.89	−5.97	−7.88	−8.08	−7.64
	ChinaSpeed	−6.25	−5.41	−5.34	−9.94	−8.84	−7.26
	SlideEditing	−1.85	−1.57	−1.51	−3.51	−3.08	−2.89
	SlideShow	−5.45	−4.88	−3.84	−8.78	−7.93	−5.32
	Average	−4.57	−4.19	−4.17	−7.52	−6.98	−5.78
	Class average	−2.80	−3.33	−4.48	−4.71	−5.27	−5.30

The highest BD-rate gains were achieved for medium- and low-resolution video test sequences (i.e., classes C and D), with average gains ranging from −3.41% to −12.82%, depending on the metric and base configuration used.

The lowest gains were obtained for class A and class E, obtaining a BD-rate gains between −1.65% and −4.01% on average.

As expected, the perceptual performance obtained by our contrast and texture masking proposals was highly dependent on the sequence type and its content but, on average, BD-rate savings of more than 5% were obtained, with particular cases achieving up to 22.89%.

As an example, the behavior of the first frame of the BQSquare sequence for all of the intra-configurations was analyzed. In Figure 12, we show the R/D curves for the first frame. As can be seen, our proposal improved the perceptual performance of the reconstructed frame for all of the metrics used. The contrast and texture masking scheme (yellow line) had the highest performance.

It is also worth noting that our proposal achieved the highest bit-rate savings at low compression rates, as can be seen in Figure 12, where for a QP of 22, we had a bit rate of 9.45 Mbps for default coding, 8.21 Mbps when contrast masking was used, and 7.72 Mbps when contrast and texture masking were used; in other words, a bit-rate saving of 18.3%.

For perceptual quality, Figure 13 compares the first frame of the BQSquare sequence encoded with $QP = 22$, whose bit-rate savings we analyzed in the previous paragraph. In this case, we compared the result of the default encoding (Figure 13a) versus the en-

coding using our proposed contrast and texture masking (Figure 13b). After performing a subjective analysis, it was quite difficult to see any difference between the two pictures.

In terms of rate distortion, our proposal managed to save a considerable number of bits at the cost of a very low perceptual quality reduction.

Table 7. Average coding performance in the random-access configuration [% BD rate].

Class	Sequence Name	Constrast Masking			Contrast and Texture Masking		
		SSIM	MS-SSIM	PSNR-HVS-M	SSIM	MS-SSIM	PSNR-HVS-M
A	Traffic	−1.60	−1.30	−2.41	−4.12	−3.87	−4.07
	PeopleOnStreet	−0.98	−0.81	−1.30	−6.38	−5.95	−4.36
	Nebuta	−2.16	−1.19	−1.55	−3.53	−2.17	−1.05
	SteamLocomotiveTrain	−0.92	−0.74	−0.93	−0.79	−0.63	−0.51
	Average	−1.42	−1.01	−1.55	−3.71	−3.15	−2.50
B	Kimono	−0.39	−0.30	−0.64	−0.75	−0.60	−0.62
	ParkScene	−2.72	−1.86	−3.30	−5.02	−4.11	−4.68
	Cactus	−3.19	−2.60	−4.75	−5.52	−4.65	−5.84
	BQTerrace	−12.00	−10.32	−12.82	−15.89	−13.59	−14.28
	BasketballDrive	−3.21	−3.20	−5.33	−6.15	−5.91	−6.59
	Average	−4.30	−3.66	−5.37	−6.67	−5.77	−6.40
C	RaceHorses	−4.48	−4.89	−6.88	−8.66	−9.00	−9.39
	BQMall	−3.31	−3.37	−4.98	−6.71	−6.76	−7.13
	PartyScene	−5.67	−5.87	−9.10	−8.56	−8.67	−10.54
	BasketballDrill	−1.61	−1.90	−3.84	−5.80	−6.01	−6.00
	Average	−3.77	−4.01	−6.20	−7.43	−7.61	−8.26
D	RaceHorses	0.60	−2.45	−4.38	−4.16	−7.38	−7.39
	BQSquare	−1.57	−8.85	−10.49	−6.29	−14.72	−13.04
	BlowingBubbles	2.21	−5.30	−9.32	−0.36	−8.32	−10.83
	BasketballPass	−1.15	−3.49	−4.60	−5.67	−8.19	−7.30
	Average	0.02	−5.02	−7.20	−4.12	−9.65	−9.64
E	FourPeople	−1.44	−1.07	−1.80	−3.33	−2.75	−2.82
	Johnny	−1.90	−1.25	−2.11	−3.72	−2.81	−2.74
	KristenAndSara	−2.37	−2.06	−2.52	−4.98	−4.42	−3.84
	Average	−1.90	−1.46	−2.15	−4.01	−3.32	−3.13
F	BasketballDrillText	−1.83	−2.15	−3.65	−6.26	−6.43	−5.90
	ChinaSpeed	−6.52	−5.88	−5.40	−11.12	−10.31	−8.08
	SlideEditing	−1.30	−0.86	−2.09	−2.19	−2.19	−3.66
	SlideShow	−4.93	−4.35	−3.89	−9.72	−8.82	−6.69
	Average	−3.64	−3.31	−3.76	−7.32	−6.94	−6.08
	Class average	−2.50	−3.08	−4.37	−5.54	−6.08	−6.00

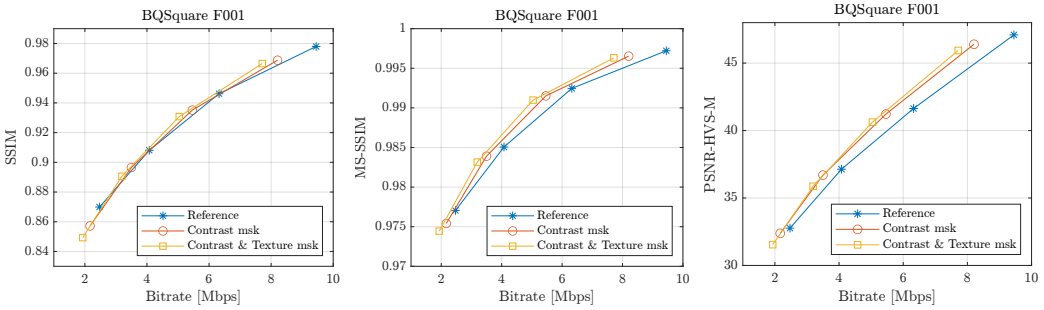

(**a**) (**b**) (**c**)

Figure 12. Rate-distortion curves of the first frame of the BQSquare sequence, comparing our proposed contrast masking (red line) and contrast and texture masking (yellow line) with the HM reference coding (blue line), using the (**a**) SSIM, (**b**) MS-SSIM, and (**c**) PSNR-HVS-M perceptual metrics.

Table 8. Average coding performance in the low-delay configuration [% BD rate].

Class	Sequence Name	Constrast Masking			Contrast and Texture Masking		
		SSIM	**MS-SSIM**	**PSNR-HVS-M**	**SSIM**	**MS-SSIM**	**PSNR-HVS-M**
A	Traffic	−1.37	−1.13	−2.40	−5.03	−4.85	−4.92
	PeopleOnStreet	−0.66	−0.72	−1.24	−6.07	−5.93	−4.33
	Nebuta	−2.29	−1.20	−1.52	−2.52	−1.37	−0.90
	SteamLocomotiveTrain	−0.71	−0.56	−0.83	−0.44	−0.07	−0.11
	Average	−1.26	−0.90	−1.50	−3.51	−3.05	−2.56
B	Kimono	−0.21	−0.16	−0.32	−0.03	0.05	0.02
	ParkScene	−1.93	−1.55	−2.67	−3.99	−3.63	−4.06
	Cactus	−2.11	−1.59	−3.68	−4.39	−3.61	−4.79
	BQTerrace	−10.42	−8.93	−13.03	−16.13	−14.36	−16.37
	BasketballDrive	−3.11	−3.08	−4.92	−6.27	−6.00	−6.52
	Average	−3.56	−3.06	−4.92	−6.16	−5.51	−6.34
C	RaceHorses	−4.27	−4.67	−7.05	−8.42	−8.82	−9.39
	BQMall	−3.36	−3.48	−5.02	−7.93	−8.01	−7.94
	PartyScene	−7.37	−7.40	−10.70	−11.57	−11.60	−13.24
	BasketballDrill	−1.13	−1.33	−2.76	−5.51	−5.69	−5.38
	Average	−4.03	−4.22	−6.38	−8.35	−8.53	−8.99
D	RaceHorses	−0.31	−2.21	−4.13	−4.99	−7.58	−6.99
	BQSquare	−8.30	−14.38	−15.77	−15.26	−22.89	−20.48
	BlowingBubbles	−2.97	−7.26	−10.74	−6.55	−11.54	−13.17
	BasketballPass	−2.64	−4.31	−5.53	−7.49	−9.55	−8.75
	Average	−3.56	−7.04	−9.04	−8.57	−12.89	−12.35
E	FourPeople	−0.20	0.01	−0.79	−2.03	−1.54	−1.20
	Johnny	−0.71	−0.35	−1.24	−4.01	−3.38	−2.99
	KristenAndSara	−1.22	−0.88	−1.45	−2.82	−2.40	−1.60
	Average	−0.71	−0.41	−1.16	−2.95	−2.44	−1.93
F	BasketballDrillText	−1.31	−1.52	−2.66	−6.28	−6.41	−5.46
	ChinaSpeed	−6.25	−5.73	−5.36	−10.81	−10.10	−7.54
	SlideEditing	−1.35	−1.48	−0.72	−3.91	−3.45	−1.99
	SlideShow	−5.59	−5.34	−5.05	−10.28	−9.75	−7.92
	Average	−3.62	−3.52	−3.45	−7.82	−7.43	−5.73
	Class average	−2.79	−3.19	−4.41	−6.23	−6.64	−6.32

(**a**) HM reference coding (9.45 Mbps)

Figure 13. *Cont*.

(**b**) Contrast and texture masking coding (7.72 Mbps)

Figure 13. Visual comparison of the first frame of the BQSquare sequence encoded at $QP = 22$. (**a**) HM reference-encoded frame; (**b**) frame encoded with contrast and texture masking.

5. Conclusions and Future Work

Compression techniques based on the HVS (e.g., texture and contrast masking) have been used for years, which proves that they are mechanisms capable of reducing the rate without impairing the image quality. In this work, we developed a novel scheme by efficiently combining contrast and texture masking techniques for the HEVC reference software showing the ability to reduce the bit rate while maintaining similar perceptual quality. We proved that by adding our proposed non-uniform 4×4 quantization matrix, we obtained an average BD-rate reduction for all of the video test sequence and the three coding modes that ranged from 2.69% (SSIM) to 4.42% (PSNR-HVS-M).

We also developed a new block classification algorithm using the mean directional variance of the image blocks and a supported vector machine, which led to a texture masking model that, in combination with contrast masking, achieved an overall average BD-rate reduction between 5.49% (SSIM) and 5.99% (MS-SSIM).

In our future work, we will (a) study the inclusion of texture over-quantization for 4×4 blocks in the HEVC reference software to further improve the RD performance of our texture masking model; (b) develop a pre-processing stage to determine when masking should not be applied at the frame level because there are sequences that hardly receive any perceptual benefit from it; and (c) evaluate other perceptual coding techniques, such as the luminance masking or the use of attention and focus metrics, which in combination with the techniques presented in this study could be able to outperform the perceptual RD performance of the HEVC reference software.

Author Contributions: Funding acquisition, O.L.-G. and G.F.E.; investigation, J.R.A., D.R.C., M.M.-R., G.V.W. and M.P.M.; software, J.R.A., D.R.C., G.F.E. and M.M.-R.; supervision, M.P.M., O.L.-G. and G.V.W.; validation, O.L.-G. and M.P.M.; writing—original draft, J.R.A., M.P.M., G.V.W., M.M.-R. and O.L.-G.; writing—review and editing, M.P.M., G.F.E., G.V.W. and O.L.-G. All authors have read and agreed to the published version of the manuscript.

Funding: This research was funded by MCIN/AEI/10.13039/501100011033 and by "ERDF A way of making Europe" under grants PID2021-123627OB-C55 and PID2021-123627OB-C52. This research was also funded by the Valencian Ministry of Innovation, Universities, Science and Digital Society (Generalitat Valenciana) under grants CIAICO/2021/278 and GV/2021/152 as well as by Junta de Comunidades de Castilla-La Mancha under grant SBPLY/21/180501/000195.

Data Availability Statement: We value reproducibility in research. Though our application is still in development, we can provide the current source code upon request. Interested researchers should contact the corresponding author(s) listed in the manuscript.

Conflicts of Interest: The authors declare no conflicts of interest.

Appendix A. Video Sequence Screenshots

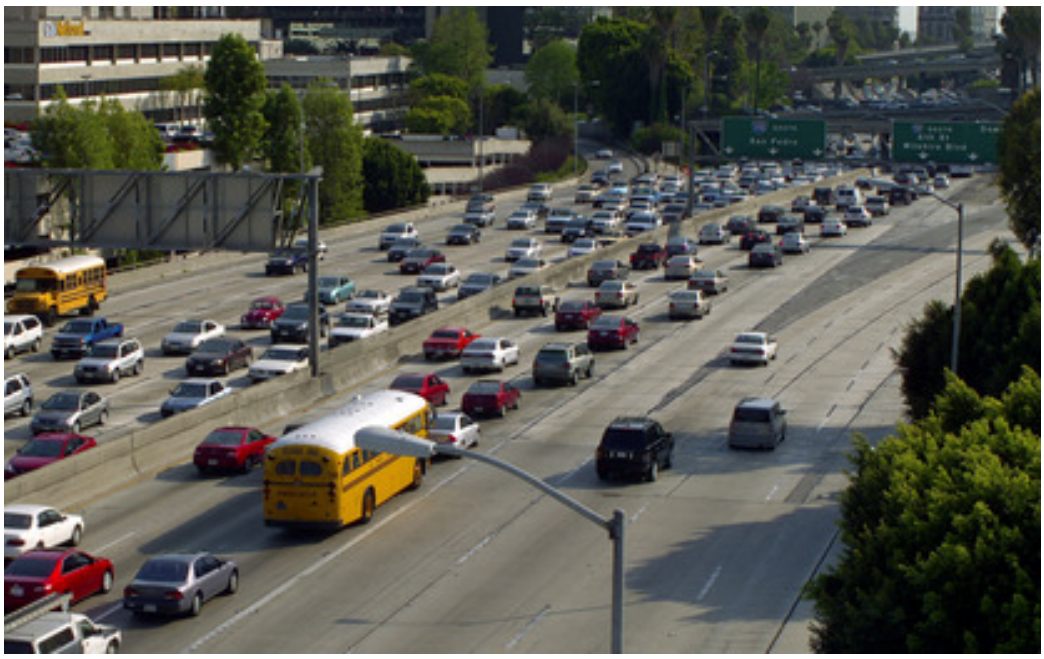

Figure A1. Traffic 2560 × 1600 30 fps Class A.

Figure A2. PeopleOnStreet 2560 × 1600 30 fps Class A.

Figure A3. NebutaFestival 2560 × 1600 60 fps Class A.

Figure A4. SteamLocomotiveTrain 2560 × 1600 60 fps Class A.

Figure A5. Kimono 1920 × 1080 24 fps Class B.

Figure A6. ParkScene 1920 × 1080 24 fps Class B.

Figure A7. Cactus 1920 × 1080 50 fps Class B.

Figure A8. BQTerrace 1920 × 1080 60 fps Class B.

Figure A9. BasketballDrive 1920 × 1080 50 fps Class B.

Figure A10. RaceHorses 832 × 480 30 fps Class C.

Figure A11. BQMall 832 × 480 60 fps Class C.

Figure A12. PartyScene 832 × 480 50 fps Class C.

Figure A13. BasketballDrill 832 × 480 50 fps Class C.

Figure A14. RaceHorses 416 × 240 30 fps Class D.

Figure A15. BQSquare 416 × 240 60 fps Class D.

Figure A16. BlowingBubbles 416 × 240 50 fps Class D.

Figure A17. BasketballPass 416 × 240 50 fps Class D.

Figure A18. FourPeople 1280 × 720 60 fps Class E.

Figure A19. Johnny 1280 × 720 60 fps Class E.

Figure A20. KristenAndSara 1280 × 720 60 fps Class E.

Figure A21. BasketballDrillText 832 × 480 50 fps Class F.

Figure A22. ChinaSpeed 1024 × 768 30 fps Class F.

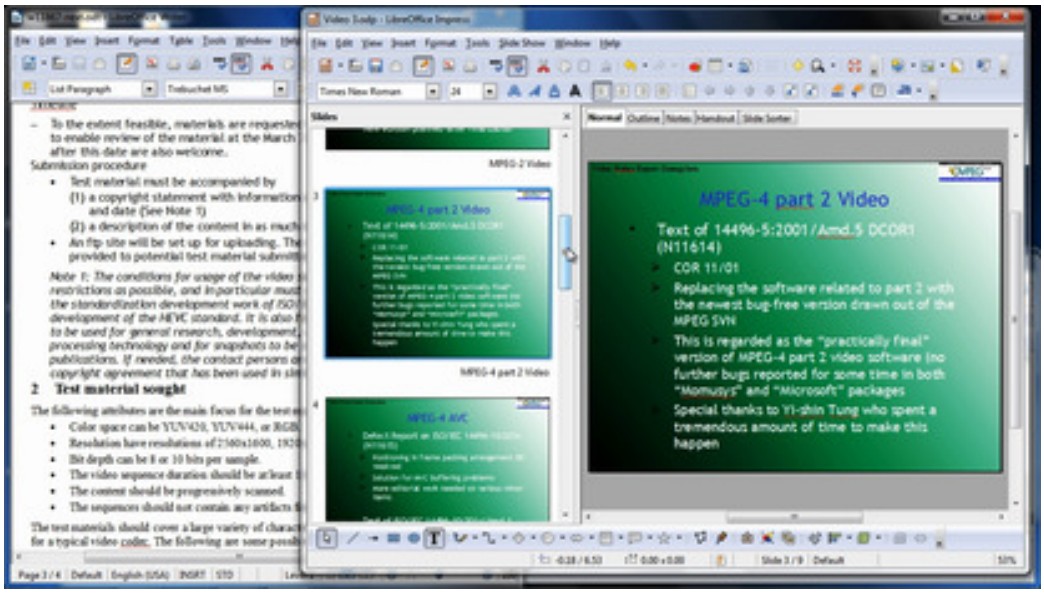

Figure A23. SlideEditing 1280 × 720 30 fps Class F.

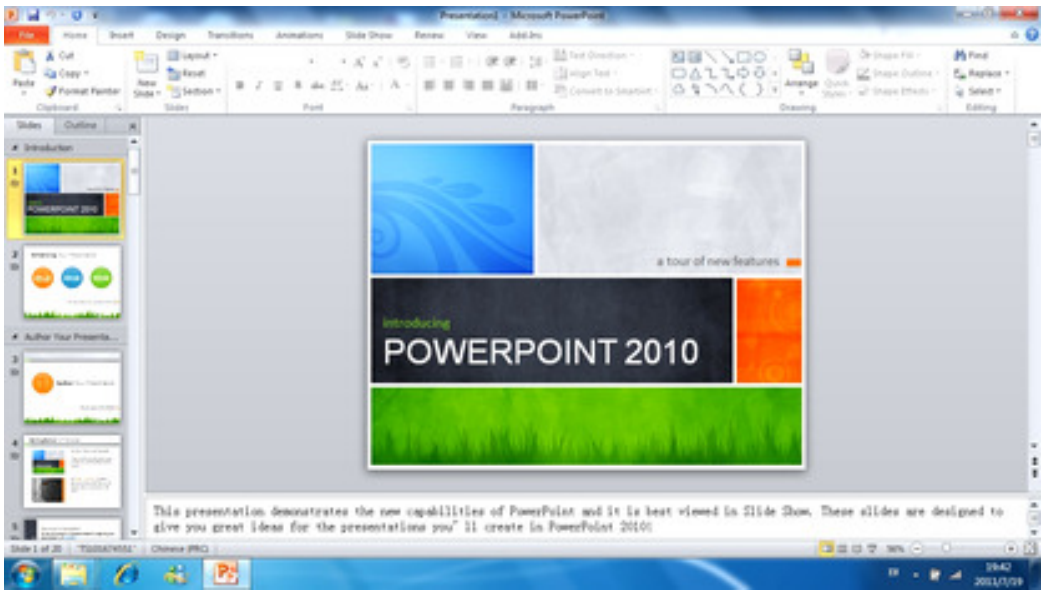

Figure A24. SlideShow 1280 × 720 20 fps Class F.

References

1. Gao, X.; Lu, W.; Tao, D.; Li, X. Image quality assessment and human visual system. In Proceedings of the Visual Communications and Image Processing 2010, Huangshan, China, 11–14 July 2010; International Society for Optics and Photonics, SPIE: San Francisco, CA, USA, 2010; Volume 7744, pp. 316–325. [CrossRef]
2. Mannos, J.; Sakrison, D. The effects of a visual fidelity criterion of the encoding of images. *IEEE Trans. Inf. Theory* **1974**, *20*, 525–536. [CrossRef]
3. Nill, N. A visual model weighted cosine transform for image compression and quality assessment. *IEEE Trans. Commun.* **1985**, *33*, 551–557. [CrossRef]
4. Daly, S. *Subroutine for the Generation of a Two Dimensional Human Visual Contrast Sensitivity Function*; Technical Report Y, 233203; Eastman Kodak: Rochester, NY, USA, 1987.
5. Ngan, K.N.; Leong, K.S.; Singh, H. Adaptive cosine transform coding of images in perceptual domain. *IEEE Trans. Acoust. Speech Signal Process.* **1989**, *37*, 1743–1750. [CrossRef]
6. Chitprasert, B.; Rao, K.R. Human visual weighted progressive image transmission. *IEEE Trans. Commun.* **1990**, *38*, 1040–1044. [CrossRef]
7. Tong, H.; Venetsanopoulos, A. A perceptual model for JPEG applications based on block classification, texture masking, and luminance masking. In Proceedings of the 1998 International Conference on Image Processing, Chicago, IL, USA, 7 October 1998; ICIP98 (Cat. No.98CB36269); Volume 3, pp. 428–432. [CrossRef]

8. *ISO/IEC 10918-1/ITU-T Recommendation T.81*; Digital Compression and Coding of Continuous-Tone Still Image. ISO: Geneva, Switzerland, 1992.
9. Zhang, X.; Lin, W.; Xue, P. Improved estimation for just-noticeable visual distortion. *Signal Process.* **2005**, *85*, 795–808. [CrossRef]
10. Wei, Z.; Ngan, K.N. Spatio-temporal just noticeable distortion profile for grey scale image/video in DCT domain. *IEEE Trans. Circuits Syst. Video Technol.* **2009**, *19*, 337–346. [CrossRef]
11. Wang, Y.; Zhang, C.; Kaithaapuzha, S. Visual Masking Model Implementation for Images & Video. In *EE368 Spring Final Paper 2009/2010*; Stanford University: Stanford, CA, USA, 2010.
12. Ma, L.; Ngan, K.N. Adaptive block-size transform based just-noticeable difference profile for videos. In Proceedings of the 2010 IEEE International Symposium on Circuits and Systems, Paris, France, 30 May–2 June 2010; pp. 4213–4216. [CrossRef]
13. Othman, Z.; Abdullah, A. An adaptive threshold based on multiple resolution levels for canny edge detection. In Proceedings of the 2nd International Conference of Reliable Information and Communication Technology (IRICT 2017), Johor, Malaysia, 23–24 April 2017; pp. 316–323. [CrossRef]
14. Gong, X.; Lu, H. Towards fast and robust watermarking scheme for H.264 Video. In Proceedings of the 2008 Tenth IEEE International Symposium on Multimedia, Berkeley, CA, USA, 15–17 December 2008; pp. 649–653. [CrossRef]
15. Mak, C.; Ngan, K.N. Enhancing compression rate by just-noticeable distortion model for H.264/AVC. In Proceedings of the 2009 IEEE International Symposium on Circuits and Systems, Taipei, Taiwan, 24–27 May 2009; pp. 609–612. [CrossRef]
16. MPEG Test Model Editing Committee. MPEG-2 Test Model 5. In Proceedings of the Sydney MPEG Meeting, Sydney, Australia, 29 March–2 April 1993.
17. Tang, C.W.; Chen, C.H.; Yu, Y.H.; Tsai, C.J. Visual sensitivity guided bit allocation for video coding. *IEEE Trans. Multimed.* **2006**, *8*, 11–18. [CrossRef]
18. McCann, K.; Rosewarne, C.; Bross, B.; Naccari, M.; Sharman, K. High Efficiency Video Coding (HEVC) Test Model 16 (HM 16) Encoder Description. In Proceedings of the 18th Meeting of the Joint Collaborative Team on Video Coding (JCT-VC), Sapporo, Japan, 30 June–7 July 2014.
19. Prangnell, L.; Hernández-Cabronero, M.; Sanchez, V. Coding block-level perceptual video coding for 4:4:4 data in HEVC. In Proceedings of the 2017 IEEE International Conference on Image Processing (ICIP), Beijing, China, 17–20 September 2017; pp. 2488–2492. [CrossRef]
20. Kim, J.; Bae, S.H.; Kim, M. An HEVC-compliant perceptual video coding scheme based on JND models for variable block-sized transform kernels. *IEEE Trans. Circuits Syst. Video Technol.* **2015**, *25*, 1786–1800. [CrossRef]
21. Wang, M.; Ngan, K.N.; Li, H.; Zeng, H. Improved block level adaptive quantization for high efficiency video coding. In Proceedings of the 2015 IEEE International Symposium on Circuits and Systems (ISCAS), Lisbon, Portugal, 24–27 May 2015; pp. 509–512. [CrossRef]
22. Xiang, G.; Jia, H.; Yang, M.; Liu, J.; Zhu, C.; Li, Y.; Xie, X. An improved adaptive quantization method based on perceptual CU early splitting for HEVC. In Proceedings of the 2017 IEEE International Conference on Consumer Electronics (ICCE), Las Vegas, NV, USA, 8–10 January 2017; pp. 362–365. [CrossRef]
23. Zhang, F.; Bull, D.R. HEVC enhancement using content-based local QP selection. In Proceedings of the 2016 IEEE International Conference on Image Processing (ICIP), Phoenix, AZ, USA, 25–28 September 2016; pp. 4215–4219. [CrossRef]
24. Marzuki, I.; Sim, D. Perceptual adaptive quantization parameter selection using deep convolutional features for HEVC encoder. *IEEE Access* **2020**, *8*, 37052–37065. [CrossRef]
25. Bosse, S.; Dietzel, M.; Becker, S.; Helmrich, C.R.; Siekmann, M.; Schwarz, H.; Marpe, D.; Wiegand, T. Neural Network Guided Perceptually Optimized Bit-Allocation for Block-Based Image and Video Compression. In Proceedings of the 2019 IEEE International Conference on Image Processing (ICIP), Taipei, Taiwan, 22–25 September 2019; pp. 126–130. [CrossRef]
26. Sanagavarapu, K.S.; Pullakandam, M. Object Tracking Based Surgical Incision Region Encoding using Scalable High Efficiency Video Coding for Surgical Telementoring Applications. *Radioengineering* **2022**, *31*, 231–242. [CrossRef]
27. Girod, B. What's Wrong with Mean-Squared Error? In *Digital Images and Human Vision*; MIT Press: Cambridge, MA, USA, 1993; pp. 207–220.
28. Eskicioglu, A.M.; Fisher, P.S. Image quality measures and their performance. *IEEE Trans. Commun.* **1995**, *43*, 2959–2965. [CrossRef]
29. Wang, Z.; Bovik, A.C.; Sheikh, H.R.; Simoncelli, E.P. Image quality assessment: From error visibility to structural similarity. *IEEE Trans. Image Process.* **2004**, *13*, 600–612. [CrossRef] [PubMed]
30. Wang, Z.; Simoncelli, E.P.; Bovik, A.C. Multiscale structural similarity for image quality assessment. In Proceedings of the Thrity-Seventh Asilomar Conference on Signals, Systems Computers, Pacific Grove, CA, USA, 9–12 November 2003; Volume 2, pp. 1398–1402. [CrossRef]
31. Ponomarenko, N.; Silvestri, F.; Egiazarian, K.; Carli, M.; Astola, J.; Lukin, V. On between-coefficient contrast masking of DCT basis functions. In Proceedings of the Third International Workshop on Video Processing and Quality Metrics, Scottsdale, AZ, USA, 25–26 January 2007; Volume 4.
32. Martínez-Rach, M.O. Perceptual Image Coding for Wavelet Based Encoders. Ph.D. Thesis, Universidad Miguel Hernández de Elche, Elche, Spain, 2014.
33. Bjontegaard, G. Calculation of average PSNR differences between RD-Curves. In Proceedings of the ITU-T Video Coding Experts Group—Thirteenth Meeting, Austin, TX, USA, 2–4 April 2001.

34. Haque, M.; Tabatabai, A.; Morigami, Y. HVS model based default quantization matrices. In Proceedings of the 7th Meeting of the Joint Collaborative Team on Video Coding (JCT-VC), Geneva, Switzerland, 21–30 November 2011.
35. Fraunhofer Institute for Telecommunications. HM Reference Software Version 16.20. 2018. Available online: https://vcgit.hhi.fraunhofer.de/jvet/HM/-/tags/HM-16.20 (accessed on 16 August 2024).
36. Bossen, F. Common test conditions and software reference. In Proceedings of the 11th Meeting of the Joint Collaborative Team on Video Coding (JCT-VC), Shanghai, China, 10–19 October 2012.
37. Atencia, J.R.; Granado, O.L.; Malumbres, M.P.; Martínez-Rach, M.O.; Van Wallendael, G. Analysis of the perceptual quality performance of different HEVC coding tools. *IEEE Access* **2021**, *9*, 37510–37522. [CrossRef]
38. Ruiz-Coll, D.; Fernández-Escribano, G.; Martínez, J.L.; Cuenca, P. Fast intra mode decision algorithm based on texture orientation detection in HEVC. *Signal Process. Image Commun.* **2016**, *44*, 12–28. [CrossRef]
39. Kundu, D.; Evans, B.L. Full-reference visual quality assessment for synthetic images: A subjective study. In Proceedings of the 2015 IEEE International Conference on Image Processing (ICIP), Quebec City, QC, Canada, 27–30 September 2015; pp. 2374–2378. [CrossRef]
40. University of Southern California, Signal and Image Processing Institute. The USC-SIPI Image Database. Available online: https://sipi.usc.edu/database/ (accessed on 5 August 2024).
41. Asuni, N.; Giachetti, A. TESTIMAGES: A large-scale archive for testing visual devices and basic image processing algorithms. In Proceedings of the Smart Tools and Apps for Graphics—Eurographics Italian Chapter Conference, Cagliari, Italy, 22–23 September 2014; Giachetti, A., Ed.; The Eurographics Association: Eindhoven, The Netherlands, 2014. [CrossRef]
42. Kodak. The Kodak Color Image Dataset. Available online: https://r0k.us/graphics/kodak/ (accessed on 16 August 2024).
43. Sze, V.; Budagavi, M.; Sullivan, G.J. *High Efficiency Video Coding (HEVC): Algorithms and Architectures*; Integrated Circuits and Systems; Springer: Berlin/Heidelberg, Germany, 2014.